Energy materials

Accelerating Li$^+$ intercalation kinetics through synergetic modification in Li-rich cathode

Jue Wu[1,*] , Zihong Chen[1], Jinqiang Cheng[1], Qiling Wen[1], Weiping Gao[1], Xianhe Wang[1], and Chao Tuo[1]

[1] *Zhuhai College of Science and Technology, Zhuhai 519041, China*

ABSTRACT

In the pursuit of high-energy density lithium-ion battery, Li-rich Mn-based oxide cathode has gained great attention with unexpectedly high capacity, low cost and excellent thermal stability. However, the cause for the sluggish kinetics remains a mystery, hindering the application of Li-rich cathode material. Here, we reveal the interfacial instability is the driving force for the sluggish kinetics, which severely blocks the interfacial Li-ion transport and triggers fast battery failure. Through rice-husk carbon (RHC) and spinel phase modification on Li-rich Mn-based oxide $Li_{1.2}Ni_{0.16}Mn_{0.56}Co_{0.08}O_2$ (LNMC), the poor lithium ion diffusion and interfacial degradation can be effectively prevented, delivering a high specific capacity of around 300 mAh/g and excellent rate performance. These findings provide a universal method to prepare high electrochemical performance Li-rich oxide materials.

Springer

GRAPHICAL ABSTRACT
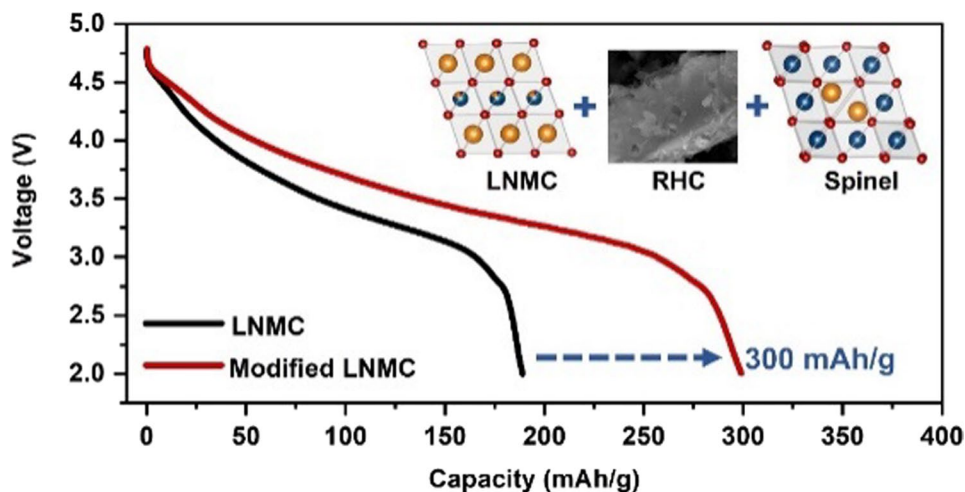
Through synergetic modification, the Li-rich Mn-based cathode delivers a high available capacity of 300 mAh/g via accelerated Li^+ intercalation kinetics

Introduction

High energy density is the pursuit of energy storage in the area of portable electronics and electric vehicles [1–3]. Li–ion battery has gained attention due to the high energy density and high conversion efficiency. Cathode material plays an important role in the development of Li-ion battery. In recent years, Li-rich cathode material has gained attention due to the high available capacity, which originated from the dual transition metal (TM) cation and oxygen anion redox reaction [4–6]. The special charge compensation mechanism for Li-rich cathode ensures high available capacity over 250 mAh/g [7, 8]. Among various Li-rich cathodes, the Li-rich Mn-based oxide cathode material has gained attention because of the abundance and low-cost of manganese elements, and high thermal stability [9].

However, poor rate performance and cycling stability limit the application of Li-rich cathode material [10, 11]. Sluggish kinetics is one of the most important reasons [12–14]. Although tremendous strategies have been developed to improve the diffusion of Li ions for Li-rich materials and remarkable progress has been achieved in Li-ion battery, most of these strategies would induce inert components at the surface of cathode material [15–18]. Besides, adopting these strategies blocks the reversibility of oxygen redox, which

decreases the available capacity [15, 19]. Hence, the critical but less solved problem lies in the interfacial Li^+ transport for Li-rich cathode composite. Eliminating Li ion diffusion kinetics could effectively boost the electrochemical performance of Li-rich oxide material. Therefore, interfacial manipulation to achieve fast interfacial kinetics could revive research into Li-rich oxide cathode and boost their electrochemical performance for practical application.

In recent years, rice-husk carbon (RHC) with good conductivity and abundant sources has been recognized as candidates of additives in energy storage device [20–22]. However, up to now, RHC has not been applied as additives in Li-rich cathode material for lithium-ion battery. Based on these, an effective engineering strategy is proposed to tailor Li-rich materials by bonding spinel phase at the surface and forming high ionic conduction pathways with RHC as the additive (Fig. 1a). Because of the *in-situ* constructing stable interface and lowered energy barrier of the charge transfer process (Fig. 1b), the synergetic modified Li-rich $Li_{1.2}Ni_{0.16}Mn_{0.56}Co_{0.08}O_2$ cathode can deliver a higher specific capacity (from 189.1 to 300.3 mAh/g), higher rate capacity (from 86.4 at 5 °C to 139.2 mAh/g at 5 °C), and excellent cycling stability. Besides, we performed the Raman, EIS and GITT test. It is demonstrated that the notable improvement in electrochemical performance lies in the stable interface

Figure 1 Schematic illustration. **a** Mechanical treatment process for pristine and modified Li-rich cathode materials (insert: layered phase and spinel phase. blue ball, Mn; red ball, O; orange ball, Li; green ball, Ni; purple ball, Co). **b** Proposed design idea to tune energy barrier of lithium-ion diffusion process via controlling surface chemistry. Sluggish interfacial kinetics due to high E_{a1} for bulk LNMC and fast interfacial kinetics with decreased E_{a2} for LNMC-RHC.
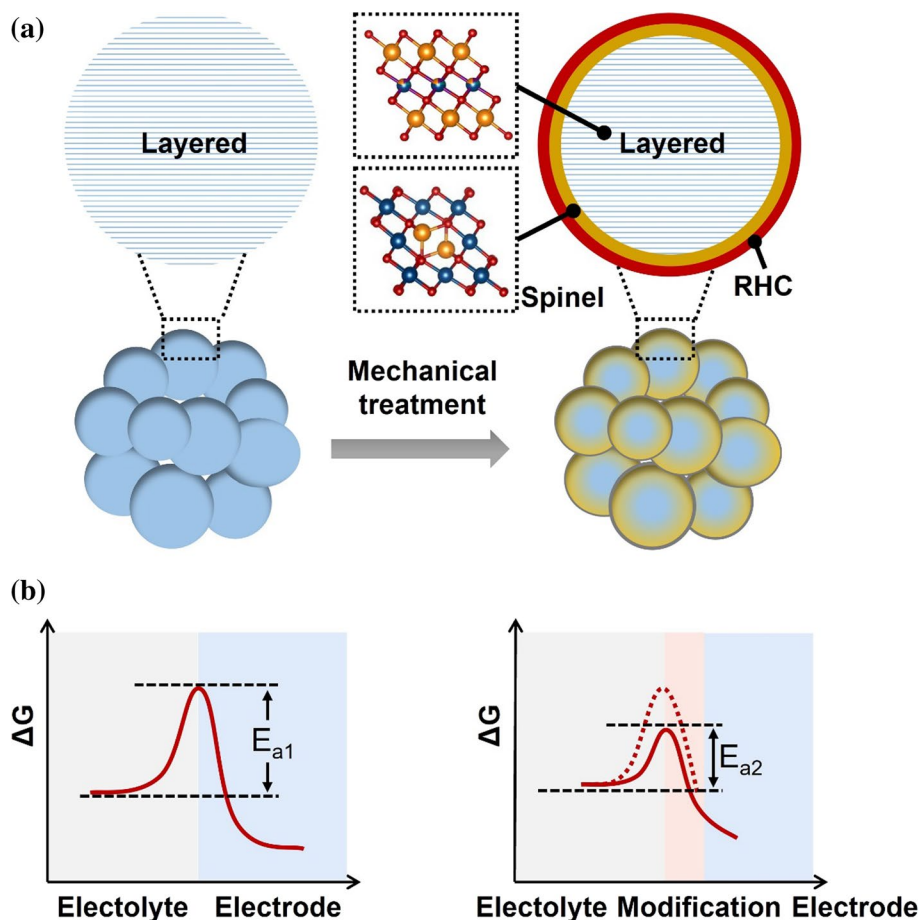
with favorable interfacial charge transfer during the cycling. This study emphasizes the importance of fast interfacial kinetics and provides a promising path for the rational design of Li-rich oxide materials to achieve high-energy density and long-term cycling stability.

Experimental

Materials synthesis

The pristine $Li_{1.2}Mn_{0.56}Ni_{0.16}Co_{0.08}O_2$ (LNMC) material was synthesized via coprecipitation–calcination method [23]. $MnSO_4 \cdot H_2O$, $NiSO_4 \cdot 6H_2O$, and $CoSO_4 \cdot 7H_2O$, and $NH_3 \cdot H_2O$ were added into a 100 mL mixed solution under the stoichiometric ratio of Mn:Ni:Co = 0.56: 0.16: 0.08, 1 mol/L NaOH solution was added and used to control the pH between 11 and 12 during the process. The as-prepared precursor was then washed with deionized water to remove any unreacted compounds, and the sample was then dried to remove water. After drying, the precursor

was mixed with Li_2CO_3 (5% excess) by ball milling. The mixture was pressed into pellets and calcined at 480 °C in air for 6 h, followed by grinding and pressing into new pellets. Finally, the new pellets were calcined at 900 °C in air for 12 h [23]. The obtained material was named as $Li_{1.2}Mn_{0.56}Ni_{0.16}Co_{0.08}O_2$ (LNMC). RHC was from Jilin Kaiyu Electrochemical Energy Storage Technologies Development Co., Ltd [22]. 0.24 g pristine LNMC was mixed with stoichiometric RHC (3 wt%, 5 wt%, 7 wt%, respectively) and acetone via mechanically ball milling. The milling process was conducted at 350 revolutions per minute (rpm) for 2 h. The obtained samples were named as LNMC-3%, LNMC-5% and LNMC-7%, respectively.

Material characterization

The XRD patterns for pristine and modified materials were obtained from X-ray diffraction (Rigaku, Japan) with Cu K_α radiation at a scanning rate of 2°/min or 10°/min between 10 and 90°. The SEM was performed (Mira, Tescan) to characterize the morphology of

materials. Raman data were collected via (LabRAM HR Evolution) in Raman shift between 200 and 900 cm^{-1} with an activated wavelength of 633 nm. The TEM experiments were conducted using JEM-2100F TEM instrument.

Electrochemical measurements

The electrochemical performance of the obtained material was measured via CR2032-type half cells. The active materials, acetylene black, and polyvinylidene fluoride (PVDF) were mixed at a weight ratio of 8:1:1 and milled with N-methyl-2-pyrrolidone (NMP) solvent to form the slurry. The slurry was then cast into the rough aluminum foils with a diameter of 12 mm and dried at 80 °C in a vacuum drying oven for over 2 h. The half cells were assembled with obtained cathode on an Ar-filled glove box, with lithium foil as the counter electrode, celgard film as the separator, the electrolyte was 1.0 M LiPF$_6$ (EC:EMC = 3:7).

Galvanostatic charge–discharge and GITT tests were conducted in a voltage window of 2.0–4.8 V using a battery testing system (T-4008 T, Neware, China). The cyclic voltammetry measurement was conducted on a CHI 660E electrochemical workstation. The EIS measurement was conducted using a multichannel potentiostat (PARSTAT MC) with a frequency from 0.01 to 100 kHz with an amplitude of 10.0 mV. For GITT analysis, the cells were cycled at the current density of 0.1 °C. The duration time for each applied galvanostatic current and rest was 10 min and 40 min, respectively.

Results and discussion

Characterization of RHC modified Li-rich oxide

The RHC modified Li-rich Li$_{1.2}$Ni$_{0.16}$Mn$_{0.56}$Co$_{0.08}$O$_2$ (LNMC-RHC) material was prepared via a facile solid-state mechanical method. The process is detailed in 'Experiment' part. The crystal structure and morphology for the pristine and RHC modified samples were recorded via X-ray diffraction (XRD) and Scanning Electron Microscopy (SEM) techniques. As shown in Fig. 2a, S1, the powder XRD patterns for pristine LNMC sample can be indexed to the layered α-NaFeO$_2$ structure (Figure S2), corresponding to the hexagonal unit cell (LiMO$_2$, M = Mn, Ni, Co, $R\bar{3}m$) and monoclinic

unit cell (Li$_2$MnO$_3$, $C2/m$) space group (the lattice order of Li and Mn, which leads to weak reflection peaks in the range of $2\theta = 20°$-25°) [19]. The diffraction peaks for LNMC-RHC materials at around 18° shift to a higher angle in the enlarged figure, indicating decreased lattice cell after RHC modification. It may be owing to the decreased Li$^+$ slab for surface spinel phase than that of layer phase, which needs further investigation. In Fig. 2b, two broad peaks were detected at around 20° and 44° for the RHC sample, suggesting disorder nature of the carbon samples [24]. The XRD patterns for LNMC-RHC materials fit well in diffraction peak (Fig. 2a), no new Bragg peak is observed, suggesting that the LNMC phases are well preserved and that RHC exists as an amorphous phase. The SEM image shows pristine LNMC sample containing uniform spherical particles with a diameter of approximately 1.0 μm (Fig. 2c).

In LNMC-5% material, the TEM result shows two sets of lattice fringes in the images. The lattice fringes in the bulk region with a d-spacing of 0.367 nm correspond to (− 111) facets of the layered structure (Fig. 2d). For the lattice fringes in the near-surface region, a new plane with a d-spacing of 0.248 nm is well consistent with the (311) facet of the spinel-like phase [25]. The TEM result suggests a spinel phase formed in the interface for LNMC-5% material. The coexistence of layered and spinel phases on the near-surface is further confirmed by Raman spectroscopy. For RHC material, some holes can be seen in the surface of particle (Fig. 2e, f).

Electrochemical performance

The prepared LNMC and LNMC-RHC samples were then assembled as coin-type cell with lithium metal as anode. The galvanostatic charge–discharge curves of pristine and modified samples were collected at a current density of 20 mA g^{-1} with a voltage window of 2.0–4.8 V versus Li/Li$^+$ (Fig. 3a). A higher specific capacity of 300.3 mAh/g is achieved for LNMC-RHC material than that of pristine LNMC material with a capacity of 189.1 mAh/g. The rate capability was evaluated at various current densities (0.2 °C, 0.5 °C, 1.0 °C, 2.0 °C, 5.0 °C, 1 °C = 200 mA/g), and then back to 0.2 °C for LNMC and LNMC-RHC material (Fig. 3b). Pristine LNMC material presents poor rate capacity, which delivers available capacity at the rate of 0.2 °C and 5 °C is 198.8 mAh/g and 86.4 mAh/g, respectively. Apparently, LNMC-5% material shows
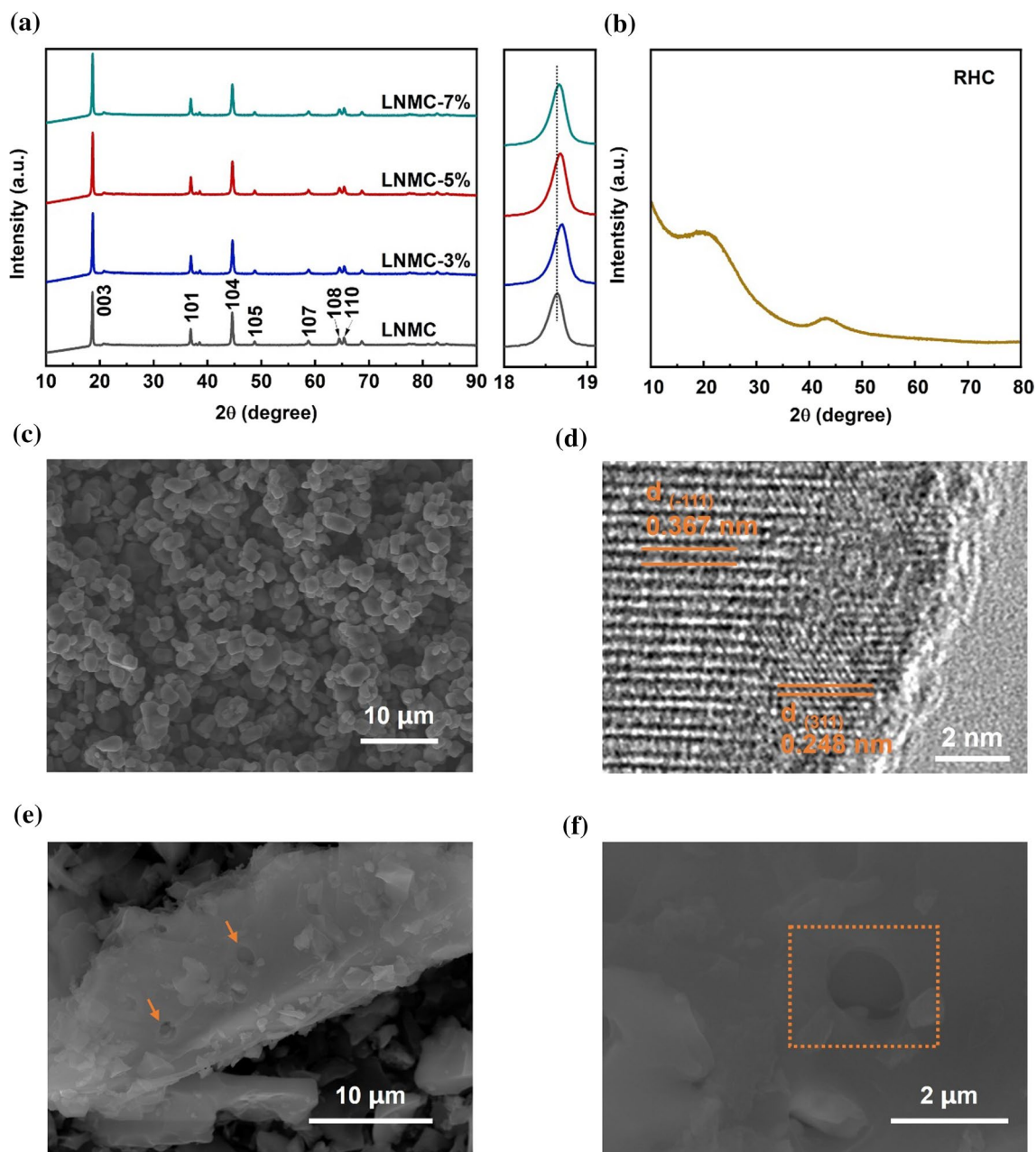
Figure 2 XRD patterns for **a** pristine and modified LNMC cathode materials (insert: enlarged area from 18.0 to 19.1 degree) and **b** raw RHC material. **c** SEM image for pristine LNMC cathode material. **d** TEM image for the interface of LNMC-5% cathode material. **e** SEM image and **f** SEM image with enlarged scale for raw RHC material.

higher discharge capacities at various current densities than pristine LNMC material. LNMC-5% can deliver around 264.5 mAh/g at the 0.2 °C rate for the first three cycles, and can deliver a capacity of 139.2 mAh/g even at a high rate of 5.0 °C. Moreover, LNMC-5% retains to 86.4% of its initial capacity when the current density backs to 0.2 °C. The data shows enhanced capacity for

RHC treated material, and the excellent capacity was maintained well at 5.0 °C and cycled back to 0.2 °C. The improved rate performance could be attributed to the accelerated Li-ion diffusion and maintained structural stability.

The curves of differential capacity over voltage (dQ/dV) were obtained from the charge–discharge profiles
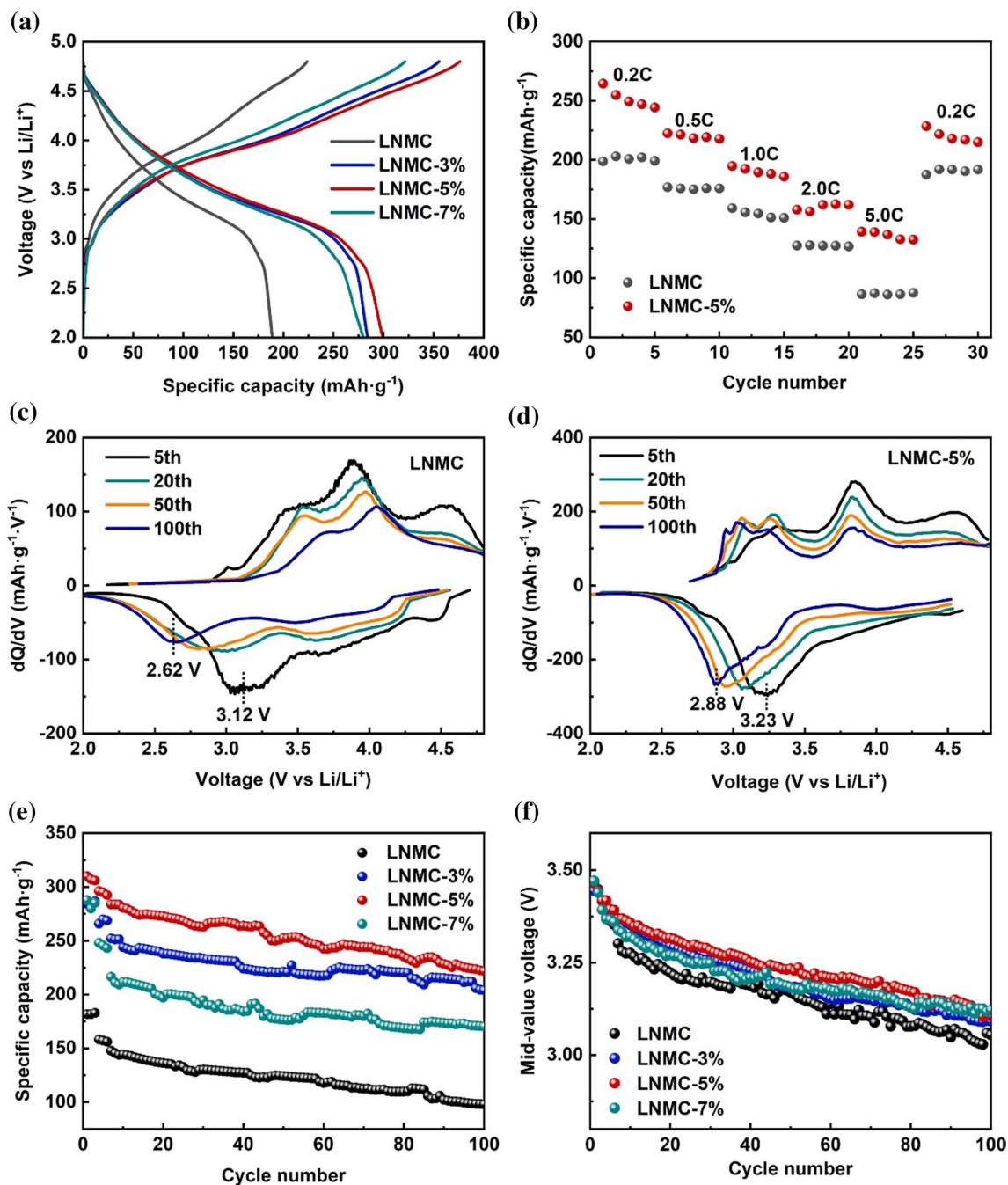
Figure 3 Electrochemical characterizations of LNMC materials. **a** The charge–discharge curves of pristine and modified LNMC materials. **b** The rate performance. **c**, **d** dQ/dV profiles for the charge–discharge processes of LNMC and LNMC-RHC materials collected from the 5th to the 100th cycle. **e** Cycling perfor-

mance comparison of pristine and modified LNMC materials at 0.1C at the first three cycles, 0.5C for three cycles and 1.0 °C for the following cycles. **f** Mid-value voltage during the cycling process for pristine and modified materials.

at the 5th, 20th, 50th and 100th cycles (Fig. 3c, d). These curves mainly possess redox couples, which relate to TM and oxygen redox [26]. The oxidation/reduction

potential difference at 3.7 V/3.8 V for the LNMC-RHC is smaller than that of the LNMC during cycles, indicating that the electrode polarization is remarkably

reduced [19]. Besides, for pristine LNMC material, the cathodic peaks continuously shift to a lower voltage (from 3.12 V for the 5th cycle to 2.62 V for the 100th cycle) and the peak intensities gradually decrease with increasing the charge–discharge cycles (Fig. 3c). Meanwhile, cathodic peaks shift in the opposite direction and are combined with decreasing peak intensity. For comparison, a decreased peak shift (from 3.23 for the 5th cycle to 2.88 V for the 100th cycle) was obtained for the modified LNMC-5% material, which suggests suppressed voltage fading for the treated sample. It is worth noting that the cathodic peaks for LNMC-5% deliver stable peak shifts, suggesting stabilized structural evolution in modified LNMC material.

Figure 3e displays the cycling performance of the electrodes for 100 cycles. The LNMC material delivers a continuous decline of discharge capacity, decreasing from 181.7 at the 1st cycle to 98.1 mAh/g at the 100th cycle when charge–discharge for 100 cycles, and with capacity retention of 54.0%. The rapid capacity decay for pristine LNMC can be ascribed to undesired side reactions [27]. LNMC exhibits the optimized cycling stability, which delivers higher discharge capacity (309.9 mAh/g at 1st to 221.8 mAh/g at 100th) during the whole cycling process with the capacity retentions of 71.6%. Figure 3f shows that the LNMC-5% exhibits better voltage stability with a mi-value voltage of 3.11 V after 100 cycles, which is higher than that of the pristine LNMC electrode. The suppressed voltage decay originates from the stabilized structural evolution, which consists with the prolonged cycling performance (Fig. 3b and e). These findings reveal that the electrochemical performance of RHC modified samples is superior to pristine LMNC material, which can mainly be attributed to action of the spinel $LiMn_2O_4$ phase on the surface of the material and the high ionic conduction pathways with RHC as the additive. It is worth noting that the discharge capacity decrease with a more heavily amount of RHC modification (LNMC-7%). A similar result, i.e., a decrease in the specific capacity was observed when Li-rich cathode material was substituted by the spinel phase [28]. This indicates that too much RHC content may inhibit the capacity release, which needs further investigation.

To understand the role of the RHC introduced on LNMC, the cell was further investigated via cyclic voltammetry (CV). Figure 4a and b show CV curves of LNMC and LNMC-5% material with different scan rates (from 0.2 to 5.0 mV s^{-1}) in the voltage range of 2.0–4.8 V [29]. As shown in CV curves, anodic peak at

around 4.0 V and cathodic peak at around 3.6 V are observed, which can be attributed to the lithium ion insertion and extraction from Li-rich materials. The peak current (I_p) increases with increased scan rate, and the cathodic peaks shift to lower potential and the anodic peaks to higher potential with the increased scan rate. Based on the Randles–Sevcik equation $\left(I_p = 2.69 \times 10^5 n^{3/2} A \left(D_{Li^+}\right)^{1/2} v^{1/2} C_{Li}\right)$, the lithium diffusion coefficient $\left(D_{Li^+}\right)$ is in proportional to the ratio of $I_p/v^{1/2}$ curve. The data show that LNMC-3% deliver higher ratio for both cathodic and anodic peak, which indicates that the RHC modified sample delivers a higher D_{Li^+} value than that of pure LMNC [30]. Impressive high D_{Li^+} in RHC can provide a fast pathway for Li ions in the RHC electrode.

To further quantify the electrode kinetics, the galvanostatic intermittent titration technique (GITT) was conducted. The GITT test was performed on coin-type cells with pristine LNMC and RHC modified electrodes at the current density of 0.1 °C with 10 min charge and 40 min relaxation for each step. Figure S3 shows GITT curves of the charge–discharge process for the pristine LNMC and LNMC-5% at the initial cycle. The overpotential values of LNMC-5% are apparently smaller than those of the pristine LNMC, suggesting that LNMC-5% possesses better Li$^+$ diffusion kinetics than the pristine LNMC. To further quantify the elevation, the chemical diffusion coefficient of lithium (D_{Li^+}) was calculated in LNMC and LNMC-RHC electrode during the charge–discharge process according to the equation in Note S1 [31]. As shown in Fig. 5a and b, it can be observed that the D_{Li^+} of LNMC-RHC is similar to the LNMC when charged to above 4.3 V and discharged to below 3.5 V. Once the voltage goes to below 4.3 V and discharged to above 3.5 V (the former range of charge or discharge), the D_{Li^+} of the LNMC-RHC is higher than that of the LNMC.

In order to study the impact of RHC coating on the charge transfer process for Li-rich oxide, the electrochemical impedance spectroscopy (EIS) was adopted to monitor cell impedance. The LNMC and LNMC-RHC materials were firstly assembled as coin-type cells and tested at pristine state [32, 33]. From the Nyquist profiles, The RCH modified materials deliver reduced semicircle in the intermediate-frequency region (Fig. 5c). The Nyquist profiles were fitted via equivalent circuit (Table S1). It is worth noting that the RHC modified material delivers charge transfer resistance (R_{ct}) with 7.18 Ω, which is lower than that
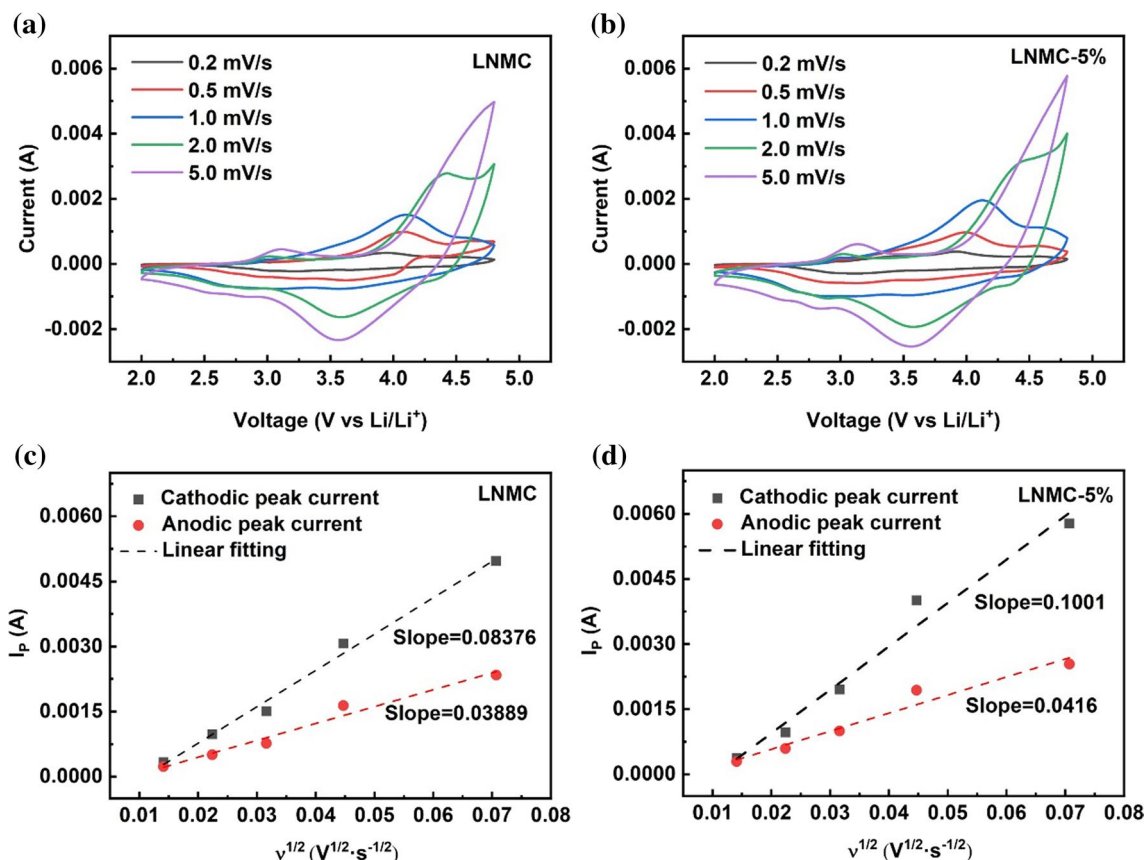
Figure 4 **a**, **b** CV profiles of the LNMC and LNMC-RHC with varying sweeping rates. **c**, **d** I_p-$v^{1/2}$ plots of the LNMC and LNMC-RHC.

of pristine LNMC with R_{ct} of 95.5 Ω. The EIS was also conducted to monitor cell impedance at varied temperatures (Figure S4). According to the Arrhenius relationship that R_{ct} follows, the value of activation energy (E_a) of the charge transfer process could be obtained from the slope of a log ($1/R_{ct}$) versus the inverse of temperature ($1/T$) plot (Table S2) [34]. As displayed in Fig. 5d, the calculated E_a for LNMC and LNMC-RHC electrodes is 29.0 kJ/mol and 15.6 kJ/mol, respectively, which means that RHC could impressively give rise to a nearly 46.2% reduction of the energy barrier for the charge transfer process [34]. The facilitated Li$^+$ transport across the electrolyte/electrode interface should be attributed to the introduction of RHC and the changed ratio of spinel phase.

The electrochemical characterizations indicate that RHC modified material exhibits lower charge transfer resistance. It is well known that the surface coating of these cathodes can result in an improvement in the electrochemistry [35]. Based on previous work [8], we can attribute this effect to a chemically modified

stable interface with RCH and spinel phase, which promote the Li$^+$ ions transport from the surface to the bulk. Thus, the RHC modification affects both the bulk and the interface of these Li-rich cathodes, resulting in their improved electrochemical performance.

Structural evolution

The XRD was conducted to monitor the structural evolution during electrochemical cycling process (Fig. 6a, b, c). In the enlarged curves (Fig. 6c), the diffraction peak positions at around 18.5° and 36.9° are shifted to lower diffraction angles for the cycled electrodes, indicating an enlarged lattice cell after electrochemical charge–discharge cycling [36]. It is worth noting that the diffraction peak at around 18.5° and 36.9° for the cycled LNMC-RHC electrode delivers a slightly lower angle than that of the LNMC electrode. Close inspection of the diffraction peak reveals that a shoulder peak appears at 43.8° (Fig. 6c), which can be indexed to the spinel phase (Figure S5). Besides, the
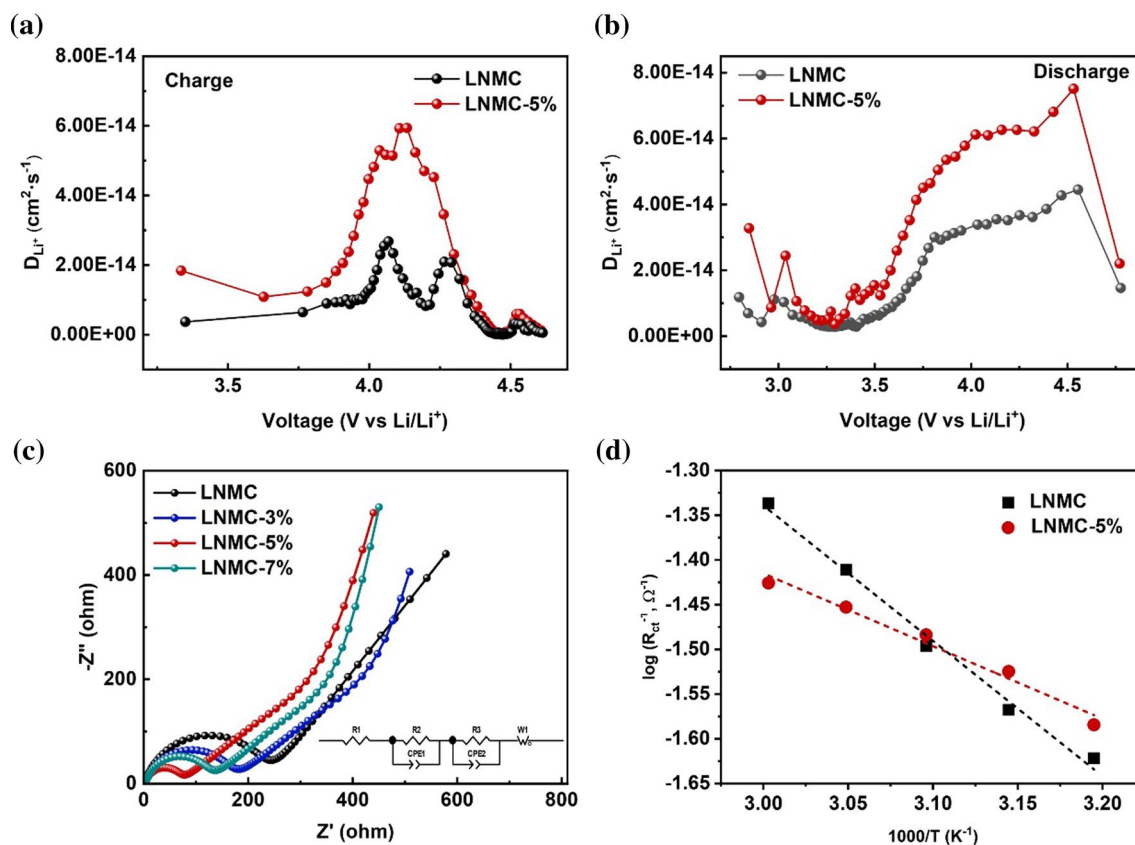
Figure 5 **a**, **b** The diffusion coefficient of lithium (D_{Li^+}) from GITT data for LNMC and LNMC-RHC materials. **c** EIS of LNMC series materials at pristine state. **d** Arrhenius plot for charge transfer resistance (R_{ct}) of LNMC without/with RHC.

main diffraction peaks for LNMC and LNMC-RHC materials at pristine and cycled states are fitted well, indicating that the structure undergoes a reversible structural transition during cycles.

Raman spectra with the pristine and cycled states for LNMC and RHC modified samples were performed to detect the surface structural evolution during electrochemical cycling process (Fig. 6d). The initial LNMC delivers a main peak at 605 cm^{-1} (black dash line) and a peak at 483 cm^{-1}, which could be described to the monoclinic Li_2MnO_3 phase [37, 38]. After long cycling (100 cycles), the new peak appears at 633 cm^{-1} (blue dash line). Compared with pristine LNMC, the treated sample delivers slowly enhanced peak at 633 cm^{-1}, indicating the existence of spinel phase [8, 39]. Besides, the RHC treated sample delivers stable peak evolution with a 605 cm^{-1} peak for both the initial and cycled samples. The Raman data suggests that the RHC treated sample delivers enhanced surface structural evolution during electrochemical cycling.

All these structural characterization results demonstrated that the introduction of spinel phase and RCH on the surface of LNMC, resulted in bulk structure well maintained.

Conclusions

In summary, Li-rich LNMC with different amounts (3%, 5%, 7%) of RHC materials were synthesized via the facial solid-state method, which introduced an *in-situ* formed spinel phase on the surface. The main phase of LNMC was well maintained after RHC coating. The detailed kinetics and mechanism studies of pristine LNMC and LNMC-RHC materials reveal that the spinel-phase covered architecture effectively facilitates the lithium ion diffusion kinetics and suppresses interfacial side reactions. Therefore, the LNMC-RHC cathode exhibits higher available capacity (300.3 mAh/g at 0.1 °C) and better rate performance (139.2 mAh/g at 5 °C, 1 A/g) than
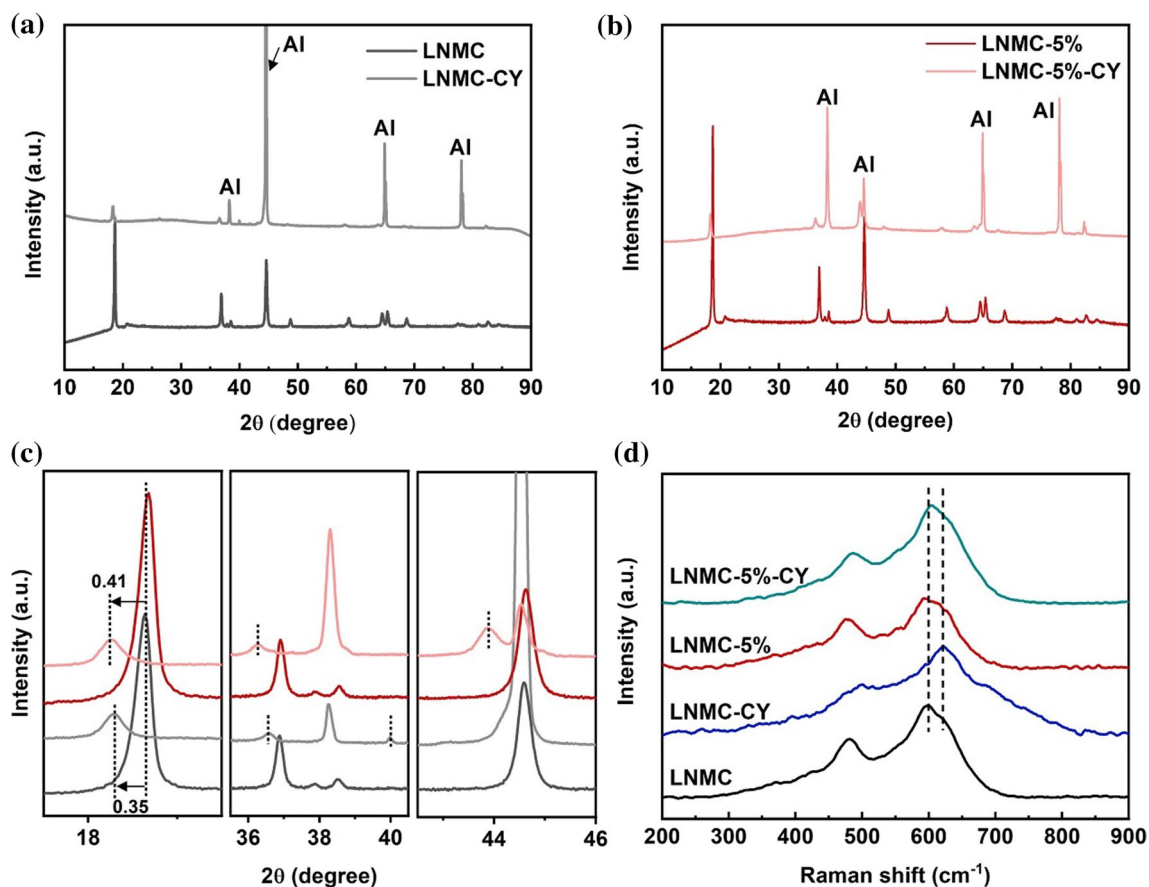
Figure 6 **a–c** The XRD data for LNMC and LNMC-RHC materials before the electrochemical cycling, and electrodes after the electrochemical cycling. **d** Raman spectra for LNMC and LNMC-RHC material.

that of pristine LNMC material (available capacity of 189.1 mAh/g at 0.1 °C, 86.4 mAh/g at 5 °C). The proposed strategy is expected to offer a simple and effective approach for Li-rich oxide to ensure power battery with high energy density and excellent rate ability.

Acknowledgements

Author contributions

JW contributed to writing–original draft, and data curation, ZC contributed to methodology, JC, QW and WG designed the study and collected the data, XW and CT analyzed the data. All authors were involved in writing and editing the manuscript.

Declarations

Conflict of interest The author declares that there is no relevant competitive economic interest or personal relationship between them that will hinder the work of this article.

Supplementary Information The online version contains supplementary material available at https://doi.org/10.1007/s10853-023-09065-3.

References

[1] Winter M, Barnett B, Xu K (2018) Before Li ion batteries. Chem Rev 118(23):11433–11456

[2] Tarascon J-M, Armand M (2011) Issues and challenges facing rechargeable lithium batteries. Nature 414(6861):359–367

[3] Goodenough JB, Kim Y (2010) Challenges for rechargeable Li batteries. Chem Mater 22(3):587–603

[4] McCalla E, Abakumov AM, Saubanère M, Foix D, Berg EJ, Rousse G, Doublet M-L, Gonbeau D, Novák P, Van Tendeloo G (2015) Visualization of O-O peroxo-like dimers in high-capacity layered oxides for Li-ion batteries. Science 350(6267):1516–1521

[5] Xu H, Guo S, Zhou H (2019) Review on anionic redox in sodium-ion batteries. J Mater Chem A 7(41):23662–23678

[6] Zuo W, Luo M, Liu X, Wu J, Liu H, Li J, Winter M, Fu R, Yang W, Yang Y (2020) Li-rich cathodes for rechargeable Li-based batteries: reaction mechanisms and advanced characterization techniques. Energy Environ Sci 13(12):4450–4497

[7] Zhang M, Liu H, Liu Z, Fang C, Meng YS (2018) Modified coprecipitation synthesis of mesostructure-controlled Li-rich layered oxides for minimizing voltage degradation. ACS Appl Energy Mater 1(7):3369–3376

[8] Wu J, Cui Z, Wu J, Xiang Y, Liu H, Zheng S, Yang W, Yang Y (2020) Suppression of voltage-decay in Li_2MnO_3 cathode via reconstruction of layered-spinel coexisting phases. J Mater Chem A 8(36):18687–18697

[9] Zhao R, Wu M, Jiao P, Wang X, Zhu J, Zhao Y, Zhang H, Zhang K, Li C, Ma Y, Chen Y (2023) A double-layer covered architecture with spinel phase induced by LiPP for Co-free Li-rich cathode with high-rate performance and long lifespan. Nano Res 16(5):6805–6814

[10] Yang W (2018) Oxygen release and oxygen redox. Nat Energy 3(8):619–620

[11] Zheng J, Myeong S, Cho W, Yan P, Xiao J, Wang C, Cho J, Zhang JG (2017) Li-and Mn-rich cathode materials: challenges to commercialization. Adv Energy Mater 7(6):1601284

[12] Sun S, Zhao CZ, Yuan H, Fu ZH, Chen X, Lu Y, Li YF, Hu JK, Dong J, Huang JQ, Ouyang M, Zhang Q (2022) Eliminating interfacial O-involving degradation in Li-rich Mn-based cathodes for all-solid-state lithium batteries. Sci Adv 8(47):eadd5189

[13] Wu Y, Zhou K, Ren F, Ha Y, Liang Z, Zheng X, Wang Z, Yang W, Zhang M, Luo M, Battaglia C, Yang W, Zhu L, Gong Z, Yang Y (2022) Highly reversible Li_2RuO_3

cathodes in sulfide-based all solid-state lithium batteries. Energy Environ Sci 15(8):3470–3482

[14] He X, Wu J, Zhu Z, Liu H, Li N, Zhou D, Zhou X, Zhang H, Bresser D, Fu Y, Crafton MJ, McCloskey BD, Chen Y, An K, Liu P, Jain A, Li J, Yang W, Yang Y, Winter M, Kostecki R (2022) Chemical and structural evolutions of Li-Mn-rich layered electrodes at different current densities. Energy Environ Sci 15(10):4137–4147

[15] Sun J, Sheng C, Cao X, Wang P, He P, Yang H, Chang Z, Yue X, Zhou H (2022) Restraining oxygen release and suppressing structure distortion in single-crystal Li-rich layered cathode materials. Adv Funct Mater 32(10):2110295

[16] Wang X, Ding Y-L, Deng Y-P, Chen Z (2020) Ni-rich/Co-poor layered cathode for automotive Li-ion batteries: promises and challenges. Adv Energy Mater 10(12):1903864

[17] Yin W, Grimaud A, Rousse G, Abakumov AM, Senyshyn A, Zhang L, Trabesinger S, Iadecola A, Foix D, Giaume D, Tarascon JM (2020) Structural evolution at the oxidative and reductive limits in the first electrochemical cycle of $Li_{1.2}Ni_{01.3}Mn_{0.54}Co_{0.13}O_2$. Nat Commun 11(1):1252–1252

[18] Zhu Z, Yu D, Yang Y, Su C, Huang Y, Dong Y, Waluyo I, Wang B, Hunt A, Yao X (2019) Gradient Li-rich oxide cathode particles immunized against oxygen release by a molten salt treatment. Nat Energy 4(12):1049–1058

[19] Meng J, Xu L, Ma Q, Yang M, Fang Y, Wan G, Li R, Yuan J, Zhang X, Yu H, Liu L, Liu T (2022) Modulating crystal and interfacial properties by W-gradient doping for highly stable and long life Li-rich layered cathodes. Adv Funct Mater 32(19):2113013

[20] Liu D, Zhang W, Lin H, Li Y, Lu H, Wang Y (2015) Hierarchical porous carbon based on the self-templating structure of rice husk for high-performance supercapacitors. RSC Adv 5(25):19294–19300

[21] Liu D, Zhang W, Lin H, Li Y, Lu H, Wang Y (2016) A green technology for the preparation of high capacitance rice husk-based activated carbon. J Clean Prod 112:1190–1198

[22] Shi J, Lin N, Wang Y, Liu D, Lin H (2020) The application of rice husk-based porous carbon in positive electrodes of lead acid batteries. J Energy Storage 30:101392

[23] Wang S, Li Y, Wu J, Zheng B, McDonald MJ, Yang Y (2015) Toward a stabilized lattice framework and surface structure of layered lithium-rich cathode materials with Ti modification. Phys Chem Chem Phys 17(15):10151–10159

[24] Kishore B, Shanmughasundaram D, Penki TR, Munichandraiah N (2014) Coconut kernel-derived activated carbon as electrode material for electrical double-layer capacitors. J Appl Electrochem 44(8):903–916

[25] Luo D, Ding X, Fan J, Zhang Z, Liu P, Yang X, Guo J, Sun S, Lin Z (2020) Accurate control of initial coulombic

efficiency for Lithium-rich manganese-based layered oxides by surface multicomponent integration. Angew Chem Int Ed 59(51):23061–23066

[26] Wei Y, Cheng J, Li D, Li Y, Zeng Z, Liu H, Zhang H, Ji F, Geng X, Lu J, Ci L (2023) A structure self-healing Li-rich cathode achieved by lithium supplement of Li-rich LLZO coating. Adv Funct Mater 33(22):2214775

[27] Wang J, He X, Paillard E, Laszczynski N, Li J, Passerini S (2016) Lithium-and manganese-rich oxide cathode materials for high-energy lithium ion batteries. Adv Energy Mater 6(21):1600906

[28] Zhang W, Sun Y, Deng H, Ma J, Zeng Y, Zhu Z, Lv Z, Xia H, Ge X, Cao S, Xiao Y, Xi S, Du Y, Cao A, Chen X (2020) Dielectric polarization in inverse spinel-structured Mg2TiO4 coating to suppress oxygen evolution of li-rich cathode materials. Adv Mater 32(19):2000496

[29] Wang C-W, Ren F-C, Zhou Y, Yan P-F, Zhou X-D, Zhang S-J, Liu W, Zhang W-D, Zou M-H, Zeng L-Y, Yao X-Y, Huang L, Li J-T, Sun S-G (2021) Engineering the interface between $LiCoO_2$ and $Li_{10}GeP_2S_{12}$ solid electrolytes with an ultrathin $Li_2CoTi_3O_8$ interlayer to boost the performance of all-solid-state batteries. Energy Environ Sci 14(1):437–450

[30] Xie J, Imanishi N, Hirano A, Takeda Y, Yamamoto O, Zhao XB, Cao GS (2010) Li-ion diffusion behavior in Sn, SnO and SnO_2 thin films studied by galvanostatic intermittent titration technique. Solid State Ionics 181(35):1611–1615

[31] Cao S, Chen J, Li H, Li Z, Guo C, Chen G, Guo X, Wang X (2023) Constructing high performance Li-rich Mn-based cathode via surface phase structure controlling and ion doping. J Power Sources 555:232398

[32] Qu X, Huang H, Wan T, Hu L, Yu Z, Liu Y, Dou A, Zhou Y, Su M, Peng X, Wu H-H, Wu T, Chu D (2022) An integrated surface coating strategy to enhance the electrochemical performance of nickel-rich layered cathodes. Nano Energy 91:106665

[33] Yang G, Pan K, Lai F, Wang Z, Chu Y, Yang S, Han J, Wang H, Zhang X, Li Q (2021) Integrated co-modification of PO43 polyanion doping and Li_2TiO_3 coating for Ni-rich layered $LiNi_{0.6}Co_{0.2}Mn_{0.2}O_2$ cathode material of Lithium-Ion batteries. Chem Eng J 421:129964

[34] Zhang W, Sun X, Tang Y, Xia H, Zeng Y, Qiao L, Zhu Z, Lv Z, Zhang Y, Ge X, Xi S, Wang Z, Du Y, Chen X (2019) Lowering charge transfer barrier of $LiMn_2O_4$ via nickel surface doping to enhance Li^+ intercalation kinetics at subzero temperatures. J Am Chem Soc 141(36):14038–14042

[35] Zhang XD, Shi JL, Liang JY, Yin YX, Zhang JN, Yu XQ, Guo YG (2018) Suppressing surface lattice oxygen release of Li-rich cathode materials via heterostructured spinel $Li_4Mn_5O_{12}$ coating. Adv Mater 30(29):1801751

[36] Shimoda K, Oishi M, Matsunaga T, Murakami M, Yamanaka K, Arai H, Ukyo Y, Uchimoto Y, Ohta T, Matsubara E, Ogumi Z (2017) Direct observation of layered-to-spinel phase transformation in Li_2MnO_3 and the spinel structure stabilised after the activation process. J Mater Chem A 5(14):6695–6707

[37] Yu F-D, Que L-F, Wang Z-B, Zhang Y, Xue Y, Liu B-S, Gu D-M (2016) Layered-spinel capped nanotube assembled 3D Li-rich hierarchitectures for high performance Li-ion battery cathodes. J Mater Chem A 4(47):18416–18425

[38] Zhang XH, Cao S, Yu RZ, Li C, Huang Y, Wang Y, Wang XY, Chen GR (2019) Improving electrochemical performances of Li-rich layered Mn-based oxide cathodes through $K_2Cr_2O_7$ solution treatment. ACS Appl Energy Mater 2(2):1563–1571

[39] Yu DYW, Yanagida K (2011) Structural analysis of Li_2MnO_3 and related Li-Mn-O materials. J Electrochem Soc 158(9):A1015